

# Continuous variable encoding by ponderomotive interaction

Stefano Pirandola, Stefano Mancini, David Vitali, and Paolo Tombesi

*Dipartimento di Fisica, Università di Camerino,  
via Madonna delle Carceri 9, I-62032 Camerino, Italy*

(Dated: May 24, 2019)

Recently it has been proposed to construct quantum error-correcting codes that embed a finite-dimensional Hilbert space in the infinite-dimensional Hilbert space of a system described by continuous quantum variables [D. Gottesman *et al.*, Phys. Rev. A **64**, 012310 (2001)]. The main difficulty of this continuous variable encoding relies on the physical generation of the quantum codewords. We show that ponderomotive interaction suffices to this end. As a matter of fact, this kind of interaction between a system and a meter causes a frequency change on the meter proportional to the position quadrature of the system. Then, a phase measurement of the meter leaves the system in an eigenstate of the stabilizer generators, provided that system and meter's initial states are suitably prepared. Here we show how to implement this interaction using either travelling or trapped atoms, and how the encoding can be performed on their motional degrees of freedom. The robustness of the codes with respect to the various experimental imperfections is then carefully analyzed.

PACS numbers: 03.67.Pp, 32.80.Lg, 03.65.Ta

## I. INTRODUCTION

Quantum information, as well as classical information, can be carried either by discrete or continuous variable (CV) systems. The latter have attracted an increasing interest during last years [1]. In particular quantum error correction (QEC) techniques have been extended to this framework in order to allow CV quantum computation [2, 3]. However, CV QEC presents some different aspects with respect to that concerning qubits. In fact, while it is reasonable to encode a qubit in a block of qubits using a QEC code protecting against a large error on a single qubit of the block, this is no more true in CV systems. In such a case, in fact, the most probable effect caused by decoherence is a small diffusion in the position and momentum of all the particles. This is just the kind of noise treated in [3] where *shift-resistant* quantum codes for qudits are suitably extended to CV systems. Gottesman *et al.* [3] also show how to implement an universal set of fault-tolerant quantum gates on the encoded qubits using linear optical operations, squeezing, homodyne detection and photon counting. The only serious limitation of the scheme is the preparation of the encoded states which ideally are non-normalizable states and therefore can only be approximated introducing an intrinsic error probability in the recovery process. Travaglione and Milburn [4] have shown that it is possible to generate such approximate states by performing a sequence of operations similar to a quantum random walk algorithm [5]. More recently, we have proposed an all-optical scheme based on the cross-Kerr interaction to realize such a code [6]. In this paper we follow the suggestion of Ref. [3] and we study a *ponderomotive* interaction [7] to embed a qubit in a CV quantum system, so that its redundancy can be used to correct errors which arise from unwanted interactions with the environment. The paper is organized as follows. In Sec. II we rapidly review some elements from Ref. [3] and we turn from an ideal situation to a more realistic one. In Secs. III and IV two different physical implementations of the CV coding schemes are proposed. Sec. V is for conclusions.

## II. ENCODED STATES

A single qubit living in a Hilbert space  $\mathcal{H}$  with basis  $\{|0\rangle, |1\rangle\}$  can be encoded into a single particle [8] in such a way that the two resulting codewords  $|\overline{0}\rangle, |\overline{1}\rangle$  provide protection against small diffusion errors in both position  $x$  and momentum  $p$  (the quantum operators obey the commutation rule  $[\hat{x}, \hat{p}] = i$  so that  $x, p$  are dimensionless quantities). The two quantum codewords  $|\overline{0}\rangle, |\overline{1}\rangle$  are the simultaneous eigenstates, with eigenvalue  $+1$  of the displacement operators  $\hat{D}_x(2\theta), \hat{D}_p(2\pi\theta^{-1})$  with  $\theta \in \mathbb{R}$ , which are also the stabilizer generators of the code [9]. These codewords are therefore invariant under the shifts  $x \rightarrow x - 2\theta$  and  $p \rightarrow p - 2\pi\theta^{-1}$ . Up to a normalization factor they are given by

$$|\overline{0}\rangle = \sum_{s=-\infty}^{+\infty} |x = 2\theta s\rangle = \sum_{s=-\infty}^{+\infty} |p = \pi\theta^{-1}s\rangle \quad (1)$$

$$|\overline{1}\rangle = \sum_{s=-\infty}^{+\infty} |x = 2\theta s + \theta\rangle = \sum_{s=-\infty}^{+\infty} (-1)^s |p = \pi\theta^{-1}s\rangle = \hat{D}_x(\theta)|\overline{0}\rangle \quad (2)$$

i.e. they are a coherent superposition of infinitely squeezed states (position eigenstates and momentum eigenstates). Each of them is a comb-state both in  $x$  and in  $p$  with equally spaced spikes ( $2\theta$  in  $x$  and  $\pi\theta^{-1}$  in  $p$ ). The codewords  $|\overline{0}\rangle, |\overline{1}\rangle$  are also eigenstates of the encoded bit-flip operator  $\bar{Z} = \hat{D}_p(\pi\theta^{-1})$ . Equivalently one can also choose the codewords  $|\pm\rangle = [|\overline{0}\rangle \pm |\overline{1}\rangle]/\sqrt{2}$  which are the eigenstates of the encoded phase-flip operator  $\bar{X} = \hat{D}_x(\theta)$  and are given by:

$$|\overline{+}\rangle = \sum_{s=-\infty}^{+\infty} |x = \theta s\rangle = \sum_{s=-\infty}^{+\infty} |p = 2\pi\theta^{-1}s\rangle \quad (3)$$

$$|\overline{-}\rangle = \sum_{s=-\infty}^{+\infty} (-1)^s |x = \theta s\rangle = \sum_{s=-\infty}^{+\infty} |p = 2\pi\theta^{-1}s + \pi\theta^{-1}\rangle. \quad (4)$$

Also these states are comb-like states both in  $x$  and in  $p$ , with equally spaced spikes ( $\theta$  in  $x$  and  $2\pi\theta^{-1}$  in  $p$ ). The four codeword states are schematically displayed in Fig. 1.

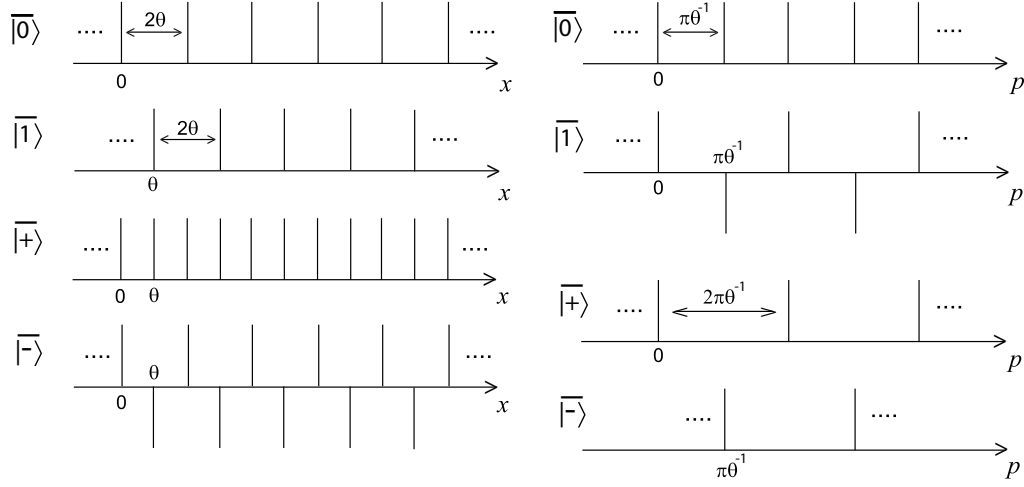


FIG. 1: Ideal encoded states  $|\overline{0}\rangle, |\overline{1}\rangle$  ( $\bar{Z}$  eigenstates) and  $|\overline{+}\rangle, |\overline{-}\rangle$  ( $\bar{X}$  eigenstates). On the left the structure of the spatial wavefunctions is displayed while on the right the structure of the momentum wavefunction is displayed. Each spike is ideally a Dirac-delta function.

The recovery process is realized by measuring the stabilizer generators  $\hat{D}_x(2\theta), \hat{D}_p(2\pi\theta^{-1})$ . The measurement of the  $X$ -generator  $\hat{D}_x(2\theta) = e^{-i2\theta\hat{p}} = \hat{p}(\text{mod } \pi\theta^{-1})$  reveals momentum shifts  $\Delta p$  which are correctable if  $|\Delta p| < \pi\theta^{-1}/2$ ; in such a case the correction is made by shifting  $p$  so to become equal to the nearest multiple of  $\pi\theta^{-1}$ . In the same way, the measurement of the  $Z$ -generator  $\hat{D}_p(2\pi\theta^{-1}) = e^{i2\pi\theta^{-1}\hat{x}} = \hat{x}(\text{mod } \theta)$  reveals position shifts which are correctable if  $|\Delta x| < \theta/2$ ; in such a case the correction is made by shifting  $x$  so to coincide with the nearest multiple of  $\theta$ .

Ref. [3] proposed the following recipe for the generation of the codeword states.

1. Preparation of a particle in the  $p = 0$  eigenstate (i.e. completely delocalized in position).
2. Coupling the particle to a meter (i.e. an oscillator, with ladder operators  $\hat{c}, \hat{c}^\dagger$ ) via the non linear interaction  $\hat{H}_{NL} = g\hat{c}^\dagger\hat{c}\hat{x}$ . This interaction modifies the frequency of the meter by  $\Delta\omega = gx$  so that, at time  $t = \pi\theta^{-1}g^{-1}$ , the phase of the meter is shifted by  $\Delta\phi = \pi\theta^{-1}x$ .
3. Reading out the phase of the meter  $\Delta\phi$  at a time  $t$ , i.e. measuring  $\hat{x}(\text{mod } 2\theta)$ . This measurement projects the initial state into a superposition of equally spaced delta function  $\delta(x - 2\theta s + \varepsilon)$  with  $s = 0, \pm 1, \dots$  and  $\varepsilon \in \mathbb{R}$ .
4. Applying a suitable transformation to obtain any desired encoded qubit state  $a|\overline{0}\rangle + b|\overline{1}\rangle$ .

Ideally the codewords are non-normalizable states infinitely squeezed both in  $x$  and  $p$ , but in practice one can only generate states with finite squeezing, i.e. only approximate codewords:  $|\widetilde{0}\rangle \sim |\overline{0}\rangle$ ,  $|\widetilde{1}\rangle \equiv \hat{D}_x(\theta)|\overline{0}\rangle \sim |\overline{1}\rangle$ ,  $|\widetilde{\pm}\rangle \equiv [|\widetilde{0}\rangle \pm |\widetilde{1}\rangle]/\mathcal{N}_\pm \sim |\pm\rangle$  ( $\mathcal{N}_\pm$  are normalization constants). For this reason, in order to estimate the quality of the encoding

scheme, together with the error probability in the recovery process due to the occurrence of an uncorrectable error, we have also to consider the *intrinsic error probability* due to the imperfections of the approximate codewords which can lead to an error even in the presence of a correctable error. Here we propose two physical implementations of the ideal coding protocol of Ref. [3], both based on single atoms interacting with a radiation mode. In general they can be derived from the ideal one by replacing the initial  $p = 0$  state with a finitely squeezed state,  $\hat{H}_{NL}$  with a ponderomotive interaction, and the phase measurement with a homodyne measurement.

### III. FLYING QUBIT SCHEME

The first coding scheme, which we shall call *flying qubit scheme*, concerns a two-level atom (or ion) transversally crossing a high finesse optical cavity and interacting with one of its modes (see Fig. 2 for a schematic description). We shall see that, if at an appropriate interaction time a homodyne measurement of an intracavity quadrature is performed, the center-of-mass motion of the atom is projected onto an approximate comb-like state, which can be used for the generation of the approximated codeword states. Notice that here we are encoding a qubit into the external degrees of freedom of a *free* atom, which can be always seen as a quantum oscillator with zero frequency.

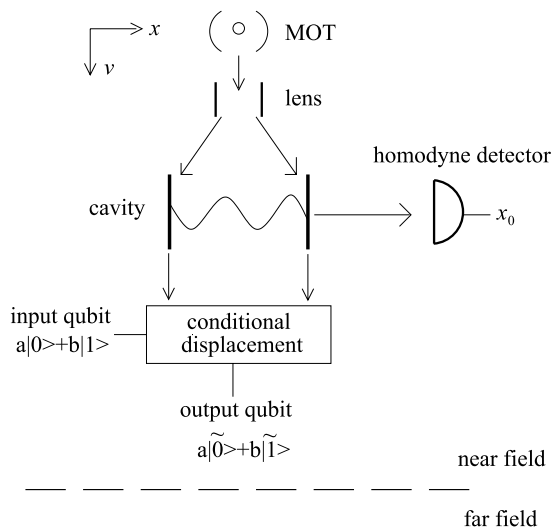


FIG. 2: *Flying qubit scheme*. An atom (or an ion) cooled in a MOT freely falls through a high finesse cavity, orthogonally to the cavity axis. Above the cavity (and relatively far from it) a diverging atomic lens causes a delocalization of the atomic wave-function entering the cavity. The atom interacts with a single mode of the cavity and after a suitable interaction time, the intracavity quadrature  $\hat{x}_0 = \hat{c} + \hat{c}^\dagger$  is measured and the atomic wave-function is projected onto an approximate comb-like state, which we take as the approximate codeword  $\tilde{|0}\rangle$ . A conditional displacement (see text) can then be used to generate any correctable state  $a\tilde{|0}\rangle + b\tilde{|1}\rangle$ .

This set-up can be realized using a small sample of atoms cooled in a magneto-optical-trap (MOT) [10] placed above the optical cavity. The atoms are then let fall down one by one through the cavity and if the MOT is distant enough from the cavity, and using appropriate collimators, the atom velocity is exactly orthogonal to the cavity axis  $x$ . We want to encode qubits into the CV corresponding to the atomic motion along  $x$  and the relevant dynamics is described (assuming, as usual in the optical domain, the rotating wave and dipole approximation) by the following Hamiltonian [11]

$$\hat{H} = \hbar\omega_0\hat{\sigma}_z + \frac{\hat{p}^2}{2M} + \hbar\omega_c\hat{c}^\dagger\hat{c} + \hbar g_0 (\hat{\sigma}^\dagger\hat{c} + \hat{c}^\dagger\hat{\sigma}) \cos k_c\hat{x}. \quad (5)$$

In this Hamiltonian  $\hat{\sigma}_z = (\hat{\sigma}^\dagger\hat{\sigma} - \hat{\sigma}\hat{\sigma}^\dagger)/2$ ,  $\hat{\sigma}, \hat{\sigma}^\dagger$  are the atomic spin-1/2 operators associated with the two internal levels whose transition is quasi-resonant with the optical cavity mode,  $\hat{x}, \hat{p}$  are the atomic center-of-mass position and momentum operators along  $x$ ,  $M$  is the atomic mass,  $\omega_0 = 2\pi c/\lambda_0$  is the atomic transition frequency ( $c$  is the speed of light),  $\hat{c}, \hat{c}^\dagger$  are the cavity mode annihilation and creation operators,  $\omega_c = ck_c = 2\pi c/\lambda_c$  is the cavity mode frequency, and  $g_0$  is the atom-field coupling constant.

A ponderomotive interaction between the atom and the cavity mode is obtained in the dispersive limit in which the cavity mode is highly (red) detuned from the atomic transition. In this limit, the upper atomic level can be adiabatically eliminated and also the spontaneous emission from it can be neglected. In such a condition the atom always remains in its ground state and the resulting ponderomotive Hamiltonian is (in a frame rotating at the frequency  $\omega_c$ )

$$\hat{H} = \frac{\hat{p}^2}{2M} - \frac{\hbar g_0^2}{\delta} \hat{c}^\dagger \hat{c} \cos^2 k_c \hat{x}, \quad (6)$$

where  $\delta \equiv \omega_0 - \omega_c$  is the detuning. We then make a second assumption, the so called Raman-Nath approximation [11], which amounts to assume that the interaction time  $t$  (given by the time the atom takes to cross the cavity mode, i.e.  $t \simeq 2w_0/v$ , where  $w_0$  is the cavity mode waist and  $v$  is the atom velocity) is short enough so that any variation of the atomic kinetic energy along  $x$  due to photon exchanges with the cavity field can be neglected. In this limit the kinetic energy along the cavity axis becomes a constant of motion, equal to its value before the cavity crossing, and therefore can be eliminated from the Hamiltonian of Eq. (6).

At the beginning the cavity mode is in a coherent state  $|\alpha\rangle_c$  (we can always choose the phase reference so that  $\alpha \geq 0$ ), while the atomic motion along the cavity axis  $x$  is described by a generic wave-function  $\Phi(x)$ , so that the initial state of the system is

$$|\Psi(0)\rangle = |\alpha\rangle_c \otimes \int dx \Phi(x) |x\rangle_a = \int dx \Phi(x) |\alpha, x\rangle. \quad (7)$$

At the end of the atom-cavity interaction, i.e. after the interaction time  $t$ , the state of the system becomes [11]

$$|\Psi(t)\rangle = e^{-\frac{i}{\hbar} \hat{H} t} |\Psi(0)\rangle = \int dx \Phi(x) |\alpha(x, t), x\rangle, \quad (8)$$

where

$$\alpha(x, t) = \alpha_1(x, t) + i\alpha_2(x, t) = \alpha \exp\left(i \frac{g_0^2 t}{\delta} \cos^2 k_c x\right). \quad (9)$$

Just at the end of the interaction we measure the intracavity quadrature  $\hat{x}_0 = \hat{c} + \hat{c}^\dagger$  [12] obtaining the result  $x_0$ . As a consequence the cavity mode is projected onto the corresponding quadrature eigenstate  $|x_0\rangle$ , while the atomic motion along  $x$  is disentangled from the cavity mode and it is projected onto the state with wave-function [11]

$$\Phi_{x_0}(x, t) = N_{x_0, t} \Phi(x) \exp\left\{-\left[\alpha_1(x, t) - \frac{x_0}{2}\right]^2 - i\alpha_2(x, t) [\alpha_1(x, t) - x_0]\right\}, \quad (10)$$

where  $N_{x_0, t}$  is a normalization constant. Now it is possible to see that this state becomes a comb-like state with well localized spikes, so that it can be used as an approximate codeword, if we choose the interaction time  $t$  where we make the homodyne measurement such that  $g_0^2 t / \delta = \pi$ , and we take as initial wave-function  $\Phi(x)$  a completely delocalized state, i.e.

$$\Phi(x) = \begin{cases} L^{-\frac{1}{2}} & 0 \leq x \leq L \\ 0 & x < 0, x > L \end{cases}, \quad (11)$$

which is an approximate momentum eigenstate with  $p = 0$  ( $L$  is the cavity length). Such a delocalized state can be prepared using a suitable diverging atomic lens, i.e. an antinode of a blue-detuned cavity or another repulsive quadratic optical potential [10, 14], soon after the MOT and before the atom enters the cavity (see Fig. 2). With the above choices, the atomic wave-function of Eq. (10) takes the following form

$$\Phi_{x_0}(x) = \begin{cases} N_{x_0} \exp\{-[\alpha_1(x) - \frac{x_0}{2}]^2 - i\alpha_2(x) [\alpha_1(x) - x_0]\} & 0 \leq x \leq L \\ 0 & x < 0, x > L \end{cases} \quad (12)$$

where  $\alpha_1(x)$  and  $\alpha_2(x)$  are given by Eq. (9) with  $g_0^2 t / \delta = \pi$  and the normalization constant  $N_{x_0}$  is given by

$$N_{x_0} = \sqrt{\frac{k_c}{d J(\alpha, x_0)}} \exp\left(\frac{x_0^2}{4}\right), \quad (13)$$

where  $d = 2L/\lambda_c$  is the integer number of half-wavelengths of the stationary cavity mode and

$$J(\alpha, x_0) \equiv \int_0^\pi dy \exp \{2\alpha_1(y) [x_0 - \alpha_1(y)]\}. \quad (14)$$

The normalization factor is connected with the probability density of the outcome  $x_0$  of the homodyne measurement, which is given by

$$\mathcal{P}(x_0) = \frac{J(\alpha, x_0)}{\sqrt{2\pi^3}} \exp\left(-\frac{x_0^2}{2}\right). \quad (15)$$

In order to make a direct comparison with the ideal codewords of Sec. II and to simplify the formulas, in the following of Sec. III we adopt dimensionless position and momentum operators by setting  $\lambda_c = \hbar = 1$ . It is also convenient to consider the scaled dimensionless position variable  $y = k_c x$ , as we have already done in Eq. (14) where  $\alpha_1(y) = \alpha_1(x = y/k_c)$ .

### A. Homodyning with a zero outcome

In order to better analyze the properties of the atomic center-of-mass states we shall use as approximate CV encoded states, we shall consider from now on the particular case of a homodyne measurement result,  $x_0 = 0$ . First of all we define the atomic state of Eq. (12) with  $x_0 = 0$ , as the approximate codeword  $|\widetilde{0}\rangle$ , i.e.

$$\varphi_0(x) \equiv \langle x | \widetilde{0} \rangle = \Phi_{x_0=0}(x) = N_0 \exp[-\alpha_1(x)^2 - i\alpha_1(x)\alpha_2(x)], \quad (0 \leq x \leq L) \quad (16)$$

where  $N_0 \equiv N_{x_0=0}$ . One can verify that the resulting wave-function  $\varphi_0(y)$  is periodic in  $0 \leq y \leq \pi d$  with period equal to  $\pi$  and it has  $2d$  equally-spaced spikes (i.e. with  $\pi/2$ -spacing, see Fig. 3(a)), so that its choice as approximate codeword state  $|\widetilde{0}\rangle$  is justified. From such a state it is easy to generate the associated codeword state  $|\widetilde{1}\rangle$  by simply displacing in  $y$  the state  $|\widetilde{0}\rangle$  by the quantity  $\pi/4$ , so that the corresponding wave-function is  $\varphi_1(y) = \varphi_0(y - \pi/4)$  (which is nonzero in  $\pi/4 \leq y \leq \pi d + \pi/4$ , see Fig. 4 for a schematic description of the corresponding probability distributions). The practical implementation of the displacement of the atomic wave-function can be easily achieved by applying, just after the cavity, a suitable uniform electric field pulse (in the case of an ion) or an electric field gradient pulse (in the case of an atom) with an appropriate intensity.

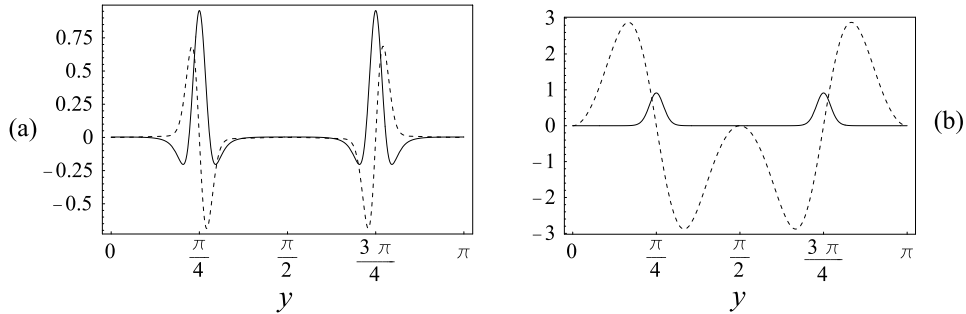


FIG. 3: Approximate codeword  $|\widetilde{0}\rangle$  corresponding to the parameters  $\alpha = 2.4$  and  $d = 20$ . In (a) the real part of the spatial wave-function  $\text{Re}\varphi_0$  (solid line) and the imaginary part  $\text{Im}\varphi_0$  (dashed line) are plotted vs the scaled position variable  $y$  inside a single period. In (b) the spatial probability distribution  $|\varphi_0|^2$  (solid line) and the phase  $-i \ln[\varphi_0/|\varphi_0|]$  (dashed line) are plotted vs the scaled position variable  $y$  inside a single period.

After seeing how the two basis codeword states are generated, let us now see how to generate a generic superposition of the two,  $a|\widetilde{0}\rangle + b|\widetilde{1}\rangle$ . These superpositions can be generated using conditional displacement schemes analogous to those used, for example, in the manipulation of quantum states of trapped ions [15] and which exploit the coupling of a motional degree of freedom with an internal transition of the ion. Schematically these schemes proceed as follows. The atom is prepared in the tensor product state  $|\widetilde{0}\rangle \otimes [a|g\rangle + b|e\rangle]$ , where  $|e\rangle$  and  $|g\rangle$  are two ground state sublevels. Then a laser pulse which is only coupled to  $|e\rangle$  is applied to the atom and its intensity is tuned so to give exactly a position shift  $y \rightarrow y - \pi/4$ . In this way the state of the atom becomes  $a|g\rangle \otimes |\widetilde{0}\rangle + b|e\rangle \otimes |\widetilde{1}\rangle$ . Then a *rf pulse* resonant with the  $e \rightarrow g$  transition and transforming  $|e\rangle \rightarrow (|e\rangle + |g\rangle)/\sqrt{2}$  and  $|g\rangle \rightarrow (|g\rangle - |e\rangle)/\sqrt{2}$  is applied, so

that the state of the atom becomes  $[|g\rangle \otimes (a|\widetilde{0}\rangle + b|\widetilde{1}\rangle) + |e\rangle \otimes (b|\widetilde{1}\rangle - a|\widetilde{0}\rangle)]/\sqrt{2}$ . When the internal state of the atom is measured and it is found equal to  $|g\rangle$ , the atomic motional state is conditionally generated in the desired encoded superposition  $a|\widetilde{0}\rangle + b|\widetilde{1}\rangle$ . Examples of superposition states are also the approximate eigenstates  $|\pm\rangle$  of the phase-flip operator  $\bar{X}$  and equivalent set of codewords, which are given by  $|\pm\rangle \equiv [|\widetilde{0}\rangle \pm |\widetilde{1}\rangle]/\mathcal{N}_\pm$ , where  $\mathcal{N}_\pm^2 = 2(1 \pm \text{Re}[\langle\widetilde{0}|\widetilde{1}\rangle])$  because  $|\widetilde{0}\rangle$  and  $|\widetilde{1}\rangle$  are not exactly orthogonal in general. Their wave-function  $\varphi_\pm(y) = [\varphi_0(y) \pm \varphi_1(y)]/\mathcal{N}_\pm$  are nonzero in  $0 \leq y \leq \pi d + \pi/4$  and have spikes spaced by  $\pi/4$ . However these approximated codewords have to be close the ideal ones also in momentum space. Performing the Fourier transform of the above wave-functions, it is possible to see that the momentum wave-function of  $|\widetilde{0}\rangle$  and  $|\widetilde{1}\rangle$ ,  $\psi_0(p)$  and  $\psi_1(p)$ , have equally spaced spikes separated by  $8\pi$ , which coincide for even  $n$  and are opposite for odd  $n$ , due to the relation  $\psi_0(p) = e^{ip/8}\psi_1(p)$ , which is an immediate consequence of the translation by  $\pi/4$  in the position coordinate. As a consequence,  $\psi_\pm(p) = [\psi_0(p) \pm \psi_1(p)]/\mathcal{N}_\pm$  have spikes spaced by  $16\pi$  and shifted by  $8\pi$  with respect to each other (see Fig. 4 (b) for a schematic representation of the probability distributions in momentum space). Therefore, from these considerations, and comparing Fig. 4 with the description of the ideal codewords states in Fig. 1, we can conclude that the states generated in the flying qubit scheme can certainly be used as approximated codeword states in the case of a spacing parameter  $\theta = 1/8$  (see Eqs.(1)-(4)). In such a case in fact, the structure of the peaks is recovered both in position and momentum space for the four codewords, even though, as expected, the approximated codewords have a finite number of peaks ( $2d$ ) and the peaks have a nonzero width and a finite height.

It is important to notice that, unfortunately, the codeword states generated in this way are not stable for a long time and therefore they can be used in a generic quantum information protocol only when the atoms are not too far from the cavity (*near field* regime). In fact, after leaving the cavity, the atomic motion along  $x$  evolves as a free particle and this evolution leads to quantum interference between the various spikes (see Ref. [11]). As we can see from Fig. 3(b), the phase change of the front of the atomic wave-function is approximately linear at the position  $y$  where  $|\varphi_0(y)|^2 \neq 0$ ; for this reason, the various spikes are deflected after the cavity and they interfere in the *far field* [11].

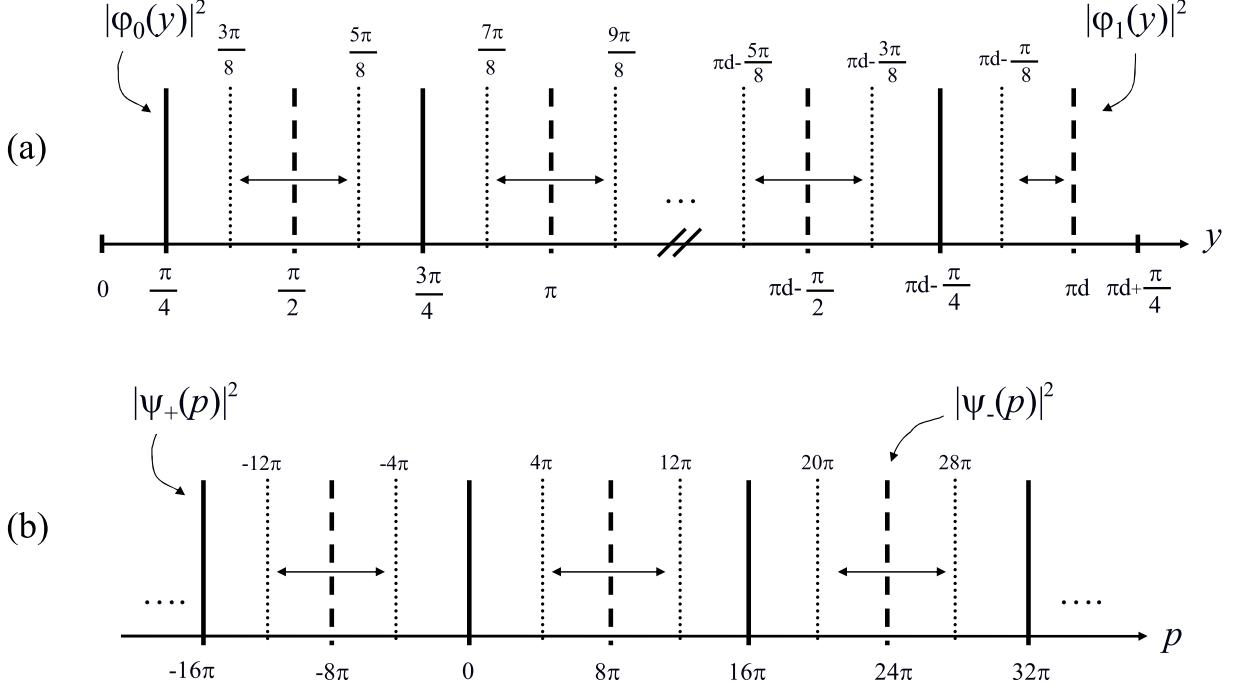


FIG. 4: **(a)** Structure of the spatial probability distributions  $|\varphi_0|^2$  (solid lines),  $|\varphi_1|^2$  (dashed lines) of the approximate codewords  $|\widetilde{0}\rangle, |\widetilde{1}\rangle$  vs the scaled variable  $y$ . The two distributions are displaced by  $\pi/4$  and each of them has  $\pi/2$ -spaced spikes. Dotted lines and arrows delimit the error regions  $R_n, R_{2d}$  defined in the text. **(b)** Structure of the momentum probability distributions  $|\psi_+(p)|^2$  (solid lines),  $|\psi_-(p)|^2$  (dashed lines) of the approximate codewords  $|\widetilde{+}\rangle, |\widetilde{-}\rangle$ . The two distributions are displaced by  $8\pi$  and each of them has  $16\pi$ -spaced spikes. Dotted lines and arrows delimit the error regions  $R_n^+$  defined in the text.

## B. Intrinsic error probability

As discussed in Sec. II, when approximated codewords are used, one has additional errors (intrinsic errors). In fact, due to the presence of the tails of the peaks, the recovery process may lead sometimes to a wrong codeword. The recovery in the spatial variable is performed by measuring the operator  $\hat{y}(\text{mod}\pi/4)$ . We can see from Fig. 4 (a) that an intrinsic error in the recovery process occurs when, given the state  $\varphi_0(y)$ , the measurement gives a result within one of the error regions:  $R_n \equiv [(4n-1)(\pi/8), (4n+1)(\pi/8)]$ ,  $n = 1, \dots, 2d-1$  and  $R_{2d} \equiv [\pi d - \pi/8, \pi d]$ . In such a case, in fact, the original state  $|0\rangle$  will be correct to the other one  $|1\rangle$  corrupting the encoded information even in the absence of any errors of the channel. The corresponding error probability  $P_{x,0}$  is equal to the one,  $P_{x,1}$ , which we would obtain starting from the state  $\varphi_1(y)$  and considering the complementary error region  $[\pi/4, \pi d] \setminus \cup_{n=1,2d} R_n$ . So, we simply have

$$P_x = \sum_{n=1}^{2d} \int_{R_n} \frac{dy}{2\pi} |\varphi_0(y)|^2 = \frac{(4d-1)N_0^2}{2\pi} \int_0^{\pi/8} dy \exp[-2\alpha_1(y)^2]. \quad (17)$$

The recovery in momentum space is done by measuring the operator  $\hat{p}(\text{mod}8\pi)$ . In the same way, one can define (see Fig. 4 (b)) the two different error regions:  $R_n^+ \equiv [(2n+1)8\pi - 4\pi, (2n+1)8\pi + 4\pi]$  and  $R_n^- \equiv [(2n)8\pi - 4\pi, (2n)8\pi + 4\pi]$  with  $n = 0, \pm 1, \dots$ . An error in the recovery process occurs when, given the state  $\psi_{\pm}(p)$ , the measurement gives a result within one of the error regions  $R_n^{\pm}$ . The corresponding error probability is then given by

$$P_{p,\pm} = \sum_{n=-\infty}^{+\infty} \int_{R_n^{\pm}} dp |\psi_{\pm}(p)|^2 = \frac{2}{N_{\pm}^2} \sum_{n=-\infty}^{+\infty} \int_{R_n^{\pm}} dp \left(1 \pm \cos \frac{p}{8}\right) |\psi_0(p)|^2. \quad (18)$$

Exploiting the parity of  $|\psi_0(p)|^2$  and the inequality (true almost everywhere)

$$|\psi_0(p)|^2 \leq \frac{4N_0^2}{\pi} \frac{\sin^2(\frac{pL}{2})}{p^2}, \quad (19)$$

we obtain

$$P_{p,+} \leq \frac{16}{\pi} \frac{N_0^2}{N_+^2} \sum_{n=0}^{+\infty} \int_{(4n+1)4\pi}^{(4n+3)4\pi} dp \left(1 + \cos \frac{p}{8}\right) \frac{\sin^2(pL/2)}{p^2} \equiv P_+, \quad (20)$$

and

$$P_{p,-} \leq \frac{8}{\pi} \frac{N_0^2}{N_-^2} \left\{ \int_{-4\pi}^{4\pi} dp \left(1 - \cos \frac{p}{8}\right) \frac{\sin^2(pL/2)}{p^2} + 2 \sum_{n=1}^{+\infty} \int_{(4n-1)4\pi}^{(4n+1)4\pi} dp \left(1 - \cos \frac{p}{8}\right) \frac{\sin^2(pL/2)}{p^2} \right\} \equiv P_-. \quad (21)$$

To estimate the quality of the overall encoding procedure provided by the present flying qubit scheme, we have to consider a mean intrinsic error probability  $\bar{P}_e$ , which is obtained in general by averaging over all the possible encoded qubit states. Using the above definitions, we have that the mean intrinsic error probability  $\bar{P}_e$  satisfies the inequality

$$\bar{P}_e \lesssim \max\{P_x, P_{p,+}, P_{p,-}\} \leq \max\{P_x, P_+, P_-\} \equiv P_{\max}, \quad (22)$$

which defines the maximum intrinsic error probability  $P_{\max}$ , providing therefore a good characterization of the proposed encoding scheme.

We have therefore to estimate  $P_{\max}$  in the case of an implementation of the flying qubit scheme on a realistic cavity QED apparatus (see for example Ref. [16]). In general the error probabilities  $P_x, P_{p,\pm}$  depend on two dimensionless parameters:  $\alpha$ , the amplitude of the initial coherent field in the cavity, and  $d$ , which is connected to the cavity length. These parameters cannot be taken at will however, because we have to satisfy the assumptions used for the derivation of the approximated codeword states, namely the large detuning and the Raman-Nath approximations. This latter approximation can also be expressed by imposing that the uncertainty of the position along the cavity axis acquired by the atom during the interaction time is much smaller than the cavity mode wavelength, i.e.  $\Delta x \ll \lambda_c$  [11] (here, we re-introduce physical dimensions, in order to fully describe the experimental implementation). One has  $\Delta p \simeq \alpha^2 \hbar k_c$  [11], from which we get  $\Delta x \simeq \Delta p t/2M \simeq \alpha^2 \hbar k_c t/2M$ , so that the Raman-Nath approximation implies the following condition on the interaction time

$$t \ll \frac{M\lambda_c^2}{\pi \hbar \alpha^2}. \quad (23)$$

On the other hand, the condition of large detuning implies  $4\alpha^2 g_0^2 / \delta^2 \ll 1$  which, together with the condition  $g_0^2 t / \delta = \pi$  used above, leads to another condition on the interaction time, i.e.

$$t \gtrsim \frac{2\pi\alpha}{g_0}, \quad (24)$$

which, combined with Eq. (23), gives the following bounds for the interaction time

$$\frac{2\pi\alpha}{g_0} \lesssim t \ll \frac{M\lambda_c^2}{\pi\hbar\alpha^2}. \quad (25)$$

This condition however puts also limitations on the possible values of  $\alpha$  and of the coupling constant  $g_0$ , which is related to the cavity mode volume  $V$  (and therefore to  $d$  because it is  $V \sim \pi w_0^2 L = \pi w_0^2 d \lambda_c / 2$ ) by the relation  $g_0 = d_{12} \sqrt{\omega_c / 2\hbar \varepsilon_0 V}$ , where  $d_{12}$  is the electric dipole matrix element associated to the atomic transition and  $\varepsilon_0$  is the vacuum dielectric constant. In order to satisfy Eq. (25) one can impose, for example,  $2\pi\alpha/g_0 = 10^{-2} M\lambda_c^2 / \pi\hbar\alpha^2$  which becomes therefore an effective relation between the two apparently independent parameters  $\alpha$  and  $d$ , which reads

$$\alpha = \sqrt[3]{\frac{g_0}{D}}, \quad D \equiv 10^2 \frac{2\pi^2 \hbar}{M\lambda_c^2}. \quad (26)$$

To state it in other words, the assumptions made in order to derive the desired encoded states implies that in practice we have only *one* free parameter, which can be  $\alpha$ ,  $d$  or the coupling constant  $g_0$ . To show the experimental feasibility of the present scheme we have considered the case of an heavy atom (*Cs*) and of an heavy ion (*Ba<sup>+</sup>*) and we have studied the behavior of the error probabilities  $P_x, P_{\pm}$  in the case of realistic parameters. In the case of *Cs* we have considered  $\lambda_0 = \lambda_c = 852.1$  nm,  $d_{12} = 3.79 \times 10^{-29}$  Cm, so that  $D \simeq 1.3 \times 10^6$  Hz, while for *Ba<sup>+</sup>* we have considered  $\lambda_0 = \lambda_c = 873.8$  nm,  $d_{12} = 5.75 \times 10^{-29}$  Cm, so that  $D \simeq 1.2 \times 10^6$  Hz.

Fig. 5 refers to *Cs* and we plot the three error probabilities and the corresponding maximum probability  $P_{max}$  as a function of the coupling constant  $g_0$  in the case of a cavity mode waist  $w_0 = 20\mu\text{m}$ . We can see that the error probabilities in position and in momentum behave in the opposite way for increasing  $g_0$  and for this reason the upper bound  $P_{max}$  has a minimum at an intermediate value  $g_0 \simeq 16$  MHz, where all the probabilities  $P_x, P_{\pm}$  have about the same order of magnitude, i.e.  $\sim 10^{-4}$ . A similar behavior is found in the case of the *Ba<sup>+</sup>* ion. In this case we do not show the behavior as a function of  $g_0$  but we simply give, as an example, a particular set of values, which are typically realized in cavity QED experiments. If we take a symmetrical near-planar resonator with curvature radius  $R = 100L$  and  $L \simeq 1.82$  mm, with waist  $w_0 = 60\mu\text{m}$ , one gets  $g_0 \simeq 13.6$  MHz, which corresponds to a remarkably small value of the intrinsic error probability,  $\bar{P}_e \lesssim 5 \times 10^{-4}$ . In such a case, the other parameters are  $\alpha \simeq 2.25$ ,  $d \simeq 4180$ ,  $\mathcal{P}(x_0 = 0) \simeq 4.7\%$ , the interaction time is  $t \simeq 10\mu\text{s}$ , and the atom velocity is  $v = 2w_0/t \simeq 10 \text{ ms}^{-1}$ .

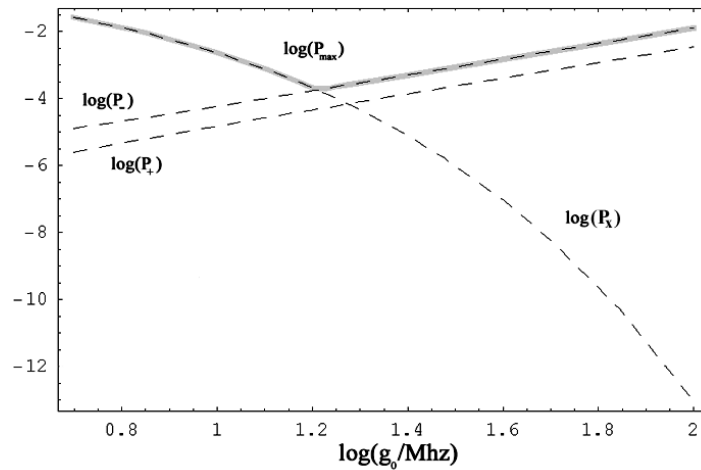


FIG. 5:  $\log_{10}(P_x)$  and  $\log_{10}(P_{\pm})$  (dashed-lines) versus  $\log_{10}(g_0/\text{MHz})$  in the case of *Cs* and for a cavity waist  $w_0 = 20\mu\text{m}$ . The quantity  $\log_{10}(P_{max})$  is the marked upper curve and it displays a minimum at about  $g_0 = 16\text{MHz}$ . In correspondence of such a minimum we have a mean error probability  $\bar{P}_e \lesssim P_{max} \sim 2 \times 10^{-4}$ .



#### IV. TRAPPED QUBIT SCHEME

The second possible implementation of the CV encoding scheme, which we call *trapped qubit scheme*, uses again a ponderomotive interaction and has some elements in common with the previous one. In fact, we consider a trapped single ion interacting with a single mode of a high-finesse cavity and an approximated codeword state is again generated in a conditional way for the center-of-mass (CM) motion of the atom when a homodyne measurement of the intracavity mode is performed (see Fig. 6 for a schematic description).

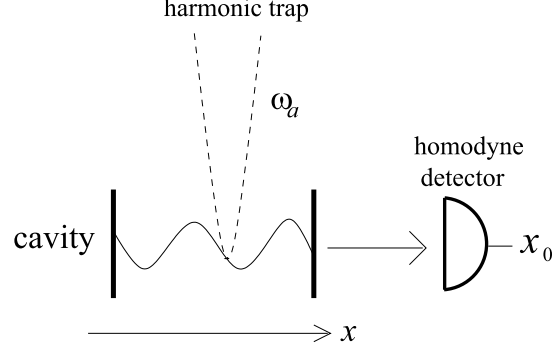


FIG. 6: *Trapped qubit scheme*. An ion is trapped by a harmonic potential within a high finesse cavity, where it interacts with a single mode. After a suitable interaction time, a homodyne measurement of the intracavity quadrature  $\hat{x}_0 = \hat{c} + \hat{c}^\dagger$  projects the state of the ion onto an approximate comb-like state, i.e. the approximate codeword  $|\widetilde{0}\rangle$ . A conditional displacement as in the previous scheme can then be used to generate any correctable state  $a|\widetilde{0}\rangle + b|\widetilde{1}\rangle$ .

To be more specific we consider a single two-level ion (with internal transition frequency  $\omega_0$ ) trapped inside a high finesse cavity by a harmonic potential, with trapping frequency  $\omega_a$  along the direction of the cavity axis  $x$  (see Ref. [17] for experimental schemes of this kind). We assume that the trapping potential in the other two directions is steep enough to freeze the motion along  $y$  and  $z$ . The ion interacts with a single cavity mode with annihilation operator  $\hat{c}$  and frequency  $\omega_c = 2\pi c/\lambda_c = ck_c$ . Therefore we have a Hamiltonian very similar to that of the preceding model (see Eq. (5)), except that we now have a non-trivial harmonic oscillator, with vibrational annihilation and creation operators  $\hat{a}, \hat{a}^\dagger$  and Hamiltonian  $\hbar\omega_a\hat{a}^\dagger\hat{a}$  instead of a free particle. If the harmonic potential minimum is set halfway in between a node and an antinode of the stationary field of the cavity mode, the system Hamiltonian can be written as

$$\hat{H} = \hbar\omega_a\hat{a}^\dagger\hat{a} + \hbar\omega_c\hat{c}^\dagger\hat{c} + \hbar\omega_0\hat{\sigma}_z + \hbar g_0 (\hat{\sigma}^\dagger\hat{c} + \hat{c}^\dagger\hat{\sigma}) \cos(k_c\hat{x} - \pi/4). \quad (27)$$

As we have seen in Sec. III, a ponderomotive interaction arises in the large detuning  $\delta = \omega_0 - \omega_c$  limit where the upper level can be adiabatically eliminated and the ion always remain in the ground state. Also in this second scheme we need another assumption, which in this case is the Lamb-Dicke limit, which amounts to assume that the ion CM is well localized with respect to a wavelength of the cavity mode  $\lambda_c$ . This assumption allows us to linearize the resulting optical potential in the far-off resonance regime. After these two approximations we get the Hamiltonian [18]

$$\hat{H} = \hbar\omega_a\hat{a}^\dagger\hat{a} + \hbar\omega_c\hat{c}^\dagger\hat{c} - \hbar g\hat{c}^\dagger\hat{c}(\hat{a} + \hat{a}^\dagger), \quad (28)$$

where  $g = (g_0^2/\delta)\xi$  and  $\xi \equiv k_c\sqrt{\hbar/2M\omega_a}$  is the Lamb-Dicke parameter. In the interaction picture with respect to  $\hat{H}_0 = \hbar\omega_c\hat{c}^\dagger\hat{c}$ , the time evolution operator assumes the form [19, 20]

$$\hat{U}(\tau) = e^{ik^2(\hat{c}^\dagger\hat{c})^2(\tau - \sin\tau)} e^{k\hat{c}^\dagger\hat{c}(\eta\hat{a}^\dagger - \eta^*\hat{a})} e^{-i\tau\hat{a}^\dagger\hat{a}}, \quad (29)$$

where  $\tau \equiv \omega_a t$ ,  $k \equiv g/\omega_a$ ,  $\eta \equiv 1 - e^{-i\tau}$ .

We consider as initial condition of the ion-cavity system the tensor product of a coherent state of amplitude  $\alpha$  for the cavity mode and a position squeezed state of amplitude  $\beta$  and squeezing parameter  $\varepsilon = r \exp\{2i\phi\}$  for the ion center of mass (see Ref. [15] for the preparation of motional squeezed states of the ion CM)

$$|\Psi(0)\rangle = |\beta, \varepsilon\rangle_a \otimes |\alpha\rangle_c, \quad |\beta, \varepsilon\rangle_a = \hat{D}(\beta) \hat{S}(\varepsilon) |0\rangle_a, \quad (30)$$

where  $\hat{D}(\beta) = \exp\{\beta\hat{a}^\dagger - \beta^*\hat{a}\}$  is the displacement operator and  $\hat{S}(\varepsilon)$  is the squeezing operator which, in the *normally-ordered* form, is given by [21]

$$\hat{S}(\varepsilon) = (\cosh r)^{-1/2} \exp\{-\Gamma\hat{a}^{\dagger 2}/2\} \exp\{-\ln(\cosh r)\hat{a}^\dagger\hat{a}\} \exp\{\Gamma^*\hat{a}^2/2\} \quad (31)$$

with  $\Gamma \equiv \exp\{2i\phi\} \tanh r$ . To compute the time-evolved state  $|\Psi(\tau)\rangle = \hat{U}(\tau)|\Psi(0)\rangle$ , we expand the optical mode coherent state  $|\alpha\rangle_c$  in number states  $|n\rangle_c$  and use the Baker-Campbell-Hausdorff expansion [22]. After some algebra, we obtain

$$|\Psi(\tau)\rangle = (\cosh r)^{-1/2} e^{-\frac{\Gamma\beta^{*2} + |\alpha|^2}{2}} \sum_{n=0}^{\infty} \frac{\alpha^n}{\sqrt{n!}} \exp[\Gamma\beta^* e^{-i\tau}(\hat{a}^\dagger - nk\eta^*) - (\Gamma/2)e^{-2i\tau}(\hat{a}^\dagger - nk\eta^*)^2 + ik^2n^2(\tau - \sin\tau)] |\beta e^{-i\tau} + nk\eta\rangle_a \otimes |n\rangle_c, \quad (32)$$

where  $|\beta e^{-i\tau} + nk\eta\rangle_a$  are coherent states of the ion CM motion. Inserting the identity decomposition in the basis of ion CM coherent states,  $\hat{I} = \int d^2\gamma |\gamma\rangle_a \langle\gamma|/\pi$  in Eq. (32), we obtain

$$|\Psi(\tau)\rangle = \mathcal{A} \sum_{n=0}^{\infty} \mathcal{B}_n \int \frac{d^2\gamma}{\pi} e^{\mathcal{C}_{n,\gamma}} |\gamma\rangle_a \otimes |n\rangle_c, \quad (33)$$

where we have defined

$$\mathcal{A} \equiv (\cosh r)^{-1/2} e^{-\frac{\Gamma\beta^{*2} + |\alpha|^2}{2}}, \quad \mathcal{B}_n \equiv \frac{\alpha^n}{\sqrt{n!}} \exp[ik^2n^2(\tau - \sin\tau) - \Gamma\zeta_n^*(\beta^* + \zeta_n^*/2) - |\beta + \zeta_n|^2/2], \quad (34)$$

$$\mathcal{C}_{n,\gamma} \equiv [\Gamma(\beta^* + \zeta_n^*) + \beta + \zeta_n]e^{-i\tau}\gamma^* - (\Gamma/2)e^{-2i\tau}\gamma^{*2} - |\gamma|^2/2, \quad \zeta_n \equiv nk(e^{i\tau} - 1). \quad (35)$$

As in the flying qubit scheme, at the (scaled) time  $\tau$  we measure the intracavity quadrature  $\hat{x}_0 = (\hat{c} + \hat{c}^\dagger)/\sqrt{2}$  obtaining the result  $x_0$ . As a consequence, the cavity mode is projected onto the corresponding quadrature eigenstate  $|x_0\rangle$ , while the ion CM motion is disentangled from the cavity mode and it is projected onto the state with wavefunction

$$\Phi(x) = \frac{N_{x_0,\tau}}{\pi^{1/4}\sqrt{1 - \Gamma e^{-2i\tau}}} \mathcal{A} \sum_{n=0}^{\infty} \langle x_0 | n \rangle_c \mathcal{B}_n e^{\mathcal{D}_n(x)}, \quad (36)$$

where  $N_{x_0,\tau}$  is a normalization constant,  $x$  is the dimensionless ion CM position  $x \rightarrow x\sqrt{M\omega_a/\hbar}$ ,

$$\mathcal{D}_n(x) \equiv \frac{(\Gamma + e^{2i\tau})x^2 + [\Gamma(\beta^* + \zeta_n^*) + \beta + \zeta_n]\{\Gamma(\beta^* + \zeta_n^*) + \beta + \zeta_n\} - 2\sqrt{2}e^{i\tau}x}{2(\Gamma - e^{2i\tau})}, \quad (37)$$

and  $\langle x_0 | n \rangle_c = \pi^{-1/4} (2^n n!)^{-1/2} H_n(x_0) e^{-x_0^2/2}$ , with  $H_n(x_0)$  the  $n^{\text{th}}$  Hermite polynomial.

### A. Homodyning with a zero outcome

We have now to determine the conditions under which the general ion CM conditional state of Eq. (36) becomes a comb-like state which can be taken as approximate codeword state. It is possible to see that one needs to choose  $k = 1/2$ , that the homodyne measurement has to be performed at the appropriate time  $\tau = \pi$ , and that initially the ion has to be displaced and squeezed in position, which is achieved if we take  $\beta, \varepsilon$  real and positive. To see this we consider again a particular example of homodyne measurement outcome, which makes things easier to see, i.e.  $x_0 = 0$ . In such a case in fact, the property  $H_{2m}(0) = (-1)^m 2^m (2m-1)!!$ ,  $H_{2m+1}(0) = 0$  ( $m = 0, 1, \dots$ ) allows to get from (36) the following expression for the ion CM wave-function

$$\varphi(x) \equiv \Phi(x)|_{k=1/2; \tau=\pi; \beta, \varepsilon \geq 0; x_0=0} = N \sum_{m=0}^{\infty} \nu_m \Omega_m(x), \quad (38)$$

where

$$\nu_m \equiv e^{-\alpha^2/2} \frac{\alpha^{2m}}{(2m)!!}, \quad \Omega_m(x) \equiv \frac{e^{r/2}}{\sqrt{\pi}} \exp\left\{-\frac{1}{2}e^{2r}[x - \sqrt{2}(2m - \beta)]^2\right\}, \quad (39)$$

(we have also taken  $\alpha$  real and positive) and  $N = [\mathcal{P}(x_0 = 0)]^{-1/2}$  with

$$\mathcal{P}(x_0 = 0) = \frac{1}{\sqrt{\pi}} \sum_{m,m'=0}^{\infty} \nu_m \nu_{m'} e^{-2e^{2r}(m-m')^2} \quad (40)$$

being the probability density corresponding to the outcome  $x_0 = 0$  of the homodyne measurement. The state of Eq. (38) represents in fact a superposition of position squeezed states centered in  $x = \sqrt{2}(2m - \beta)$ , ( $m = 0, 1, 2, \dots$ ), which is however also a superposition of squeezed states in the momentum space  $p$ , as one can verify by computing the Fourier transform

$$\psi(p) = \frac{1}{\sqrt{2\pi}} \int \varphi(x) e^{-ipx} dx = \frac{N}{\sqrt{\pi}} \exp[-(r + e^{-2r}p^2)/2] \sum_{m=0}^{\infty} \nu_m e^{-i\sqrt{2}p(2m-\beta)} \quad (41)$$

(see Figs. 7(a), 7(e), 7(g)). Therefore, also in the present scheme, the homodyne measurement of the cavity mode conditionally generates the desired comb-like state, which we can take as the approximate codeword state  $|\widetilde{0}\rangle$ . This state depends upon the three dimensionless parameters  $\alpha$ ,  $\beta$ , and  $r$ . The parameter  $r$  is obviously responsible for squeezing in  $x$  and increases the number of spikes in  $p$  (as we can see from Eqs. (39), and (41)), while  $\alpha$  causes squeezing in  $p$  and increases the number of spikes in  $x$ . This fact can be seen if we consider the probability to have the  $m^{th}$  spike  $\Omega_m(x)$  in the wave-function  $\varphi(x)$ ,  $P(m) = \nu_m / \sum_{m=0}^{\infty} \nu_m$ . In fact one can see that the mean value  $\bar{m}$  and its standard deviation  $\Delta m$  are approximately given by

$$\bar{m} \simeq \alpha^2/2, \quad \Delta m \simeq \alpha/\sqrt{2}, \quad (42)$$

implying that the number of spikes in  $x$  grows linearly with  $\alpha$ . These arguments shows that the generated approximate comb-like state approaches the ideal codeword state  $|0\rangle$  of Sec. II for  $\alpha, r \rightarrow \infty$  and that we have to take these latter parameters as large as possible. By varying the parameter  $\beta$  instead, one simply shifts the state along  $x$ .

Therefore, by comparing with the ideal codeword state of Eq. (1), we have that the state of Eq. (38) approximates it (except for an unimportant shift by  $\beta$ ) with  $\theta = \sqrt{2}$ . The other three important codeword states  $|\widetilde{1}\rangle$ ,  $|\widetilde{+}\rangle$ , and  $|\widetilde{-}\rangle$  of Eqs. (2)-(4) can be approximated starting from  $|\widetilde{0}\rangle$  and following the same strategy adopted in the flying qubit case. This means that the approximate codeword  $|\widetilde{1}\rangle \equiv \hat{D}_x(-\sqrt{2})|\widetilde{0}\rangle$  is generated by a position shift equivalent to a change of the parameter  $\beta$ ,  $\Delta\beta = 1$ , and which can be again realized by applying a suitable electric field (or laser) pulse (see Ref. [15]). Moreover, the generic encoded superposition  $a|\widetilde{0}\rangle + b|\widetilde{1}\rangle$  can be generated as well by adopting the same conditional displacement scheme outlined in Sec. III for the flying qubit scheme. Particular examples of these superpositions are the eigenstates of the encoded phase-flip operator  $\widetilde{X}$ , whose approximate versions are given by  $|\widetilde{\pm}\rangle \equiv [|\widetilde{0}\rangle \pm |\widetilde{1}\rangle]/\mathcal{N}_{\pm}$ , where  $\mathcal{N}_{\pm}^2 = 2[1 \pm \langle\widetilde{0}|\widetilde{1}\rangle]$  ( $|\widetilde{0}\rangle$  and  $|\widetilde{1}\rangle$  are not orthogonal in general also in this scheme). It is interesting to notice that the corresponding wave-functions of these latter codeword states  $|\widetilde{\pm}\rangle$  in the momentum space are given by

$$\psi_{\pm}(p) \equiv \langle p | \widetilde{\pm} \rangle = \frac{N}{\pi^{1/2}\mathcal{N}_{\pm}} e^{i\sqrt{2}\beta p - (r + e^{-2r}p^2)/2} (1 \pm e^{i\sqrt{2}p}) \sum_{m=0}^{\infty} \nu_m e^{-i\sqrt{2}mp} \quad (43)$$

showing that  $|\psi_+(p)|^2$  has spikes at  $p_n = \pi(2n)/\sqrt{2}$  while  $|\psi_-(p)|^2$  has spikes at  $p_n = \pi(2n+1)/\sqrt{2}$ . ( $n = 0, \pm 1, \dots$ ) (see Fig. 7(d)). See Fig. 7(a)-7(h) for plots of the spatial and momentum wave-functions of the various approximate codewords  $|\widetilde{0}\rangle, |\widetilde{1}\rangle, |\widetilde{+}\rangle, |\widetilde{-}\rangle$  in the case  $\beta = 0$  and for the particular values  $\alpha = 1.8$  and  $r = 1.5$ .

## B. Intrinsic error probability

From the point of view of the recovery, the situation is similar to the one depicted in Fig. 4 and treated in Sec. III B, with the only difference that we have  $\theta = \sqrt{2}$  instead of  $\theta = 1/8$  and we have in general a position shift by  $-\beta\sqrt{2}$ . The recovery in the spatial variable is performed by measuring the operator  $(\hat{x} + \beta\sqrt{2})(\text{mod}\sqrt{2})$ . An intrinsic error in the

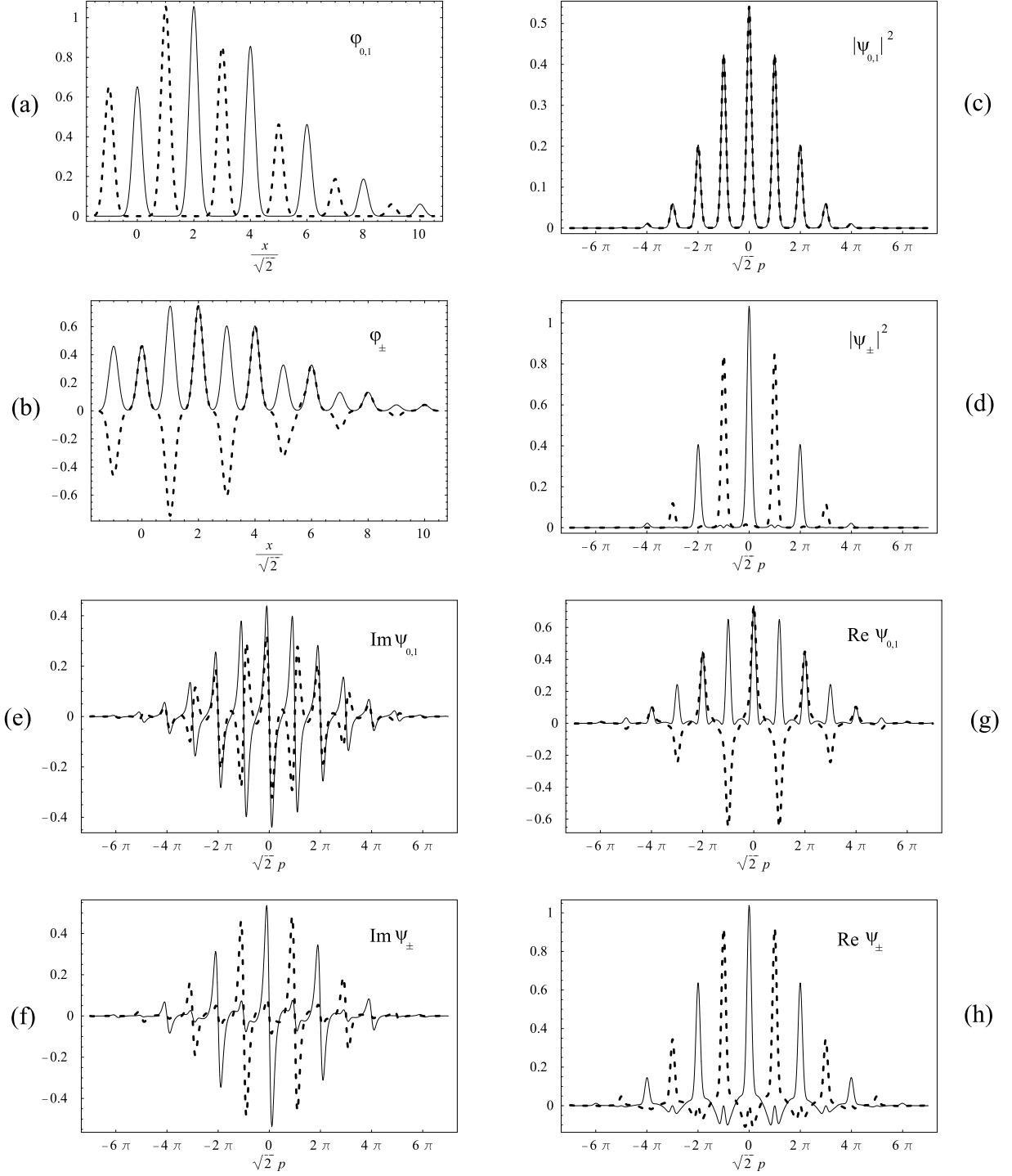


FIG. 7: Plot of the wave-functions in space and momentum coordinates of the approximate codeword states  $\widetilde{|0\rangle}$ ,  $\widetilde{|1\rangle}$ ,  $\widetilde{|+\rangle}$  and  $\widetilde{|-\rangle}$  for  $\alpha = 1.8$ ,  $r = 1.5$  and  $\beta = 0$ . (a): spatial wave-functions  $\phi_0$  of  $\widetilde{|0\rangle}$  (solid line) and  $\phi_1$  of  $\widetilde{|1\rangle}$  (dashed line) vs  $x/\sqrt{2}$ ; (b): spatial wave-functions  $\phi_+$  of  $\widetilde{|+\rangle}$  (solid line) and  $\phi_-$  of  $\widetilde{|-\rangle}$  (dashed line) vs  $x/\sqrt{2}$ ; (c): momentum probability distributions  $|\psi_0|^2$  of  $\widetilde{|0\rangle}$  (solid line) and  $|\psi_1|^2$  of  $\widetilde{|1\rangle}$  (dashed line) vs  $\sqrt{2}p$ ; (d): momentum probability distributions  $|\psi_+|^2$  of  $\widetilde{|+\rangle}$  (solid line) and  $|\psi_-|^2$  of  $\widetilde{|-\rangle}$  (dashed line) vs  $\sqrt{2}p$ ; (e): imaginary part of the momentum wave-functions  $\text{Im } \psi_0$  of  $\widetilde{|0\rangle}$  (solid line) and  $\text{Im } \psi_1$  of  $\widetilde{|1\rangle}$  (dashed line) vs  $\sqrt{2}p$ ; (f): imaginary part of the momentum wave-functions  $\text{Im } \psi_+$  of  $\widetilde{|+\rangle}$  (solid line) and  $\text{Im } \psi_-$  of  $\widetilde{|-\rangle}$  (dashed line) vs  $\sqrt{2}p$ ; (g): real part of the momentum wave-functions  $\text{Re } \psi_0$  of  $\widetilde{|0\rangle}$  (solid line) and  $\text{Re } \psi_1$  of  $\widetilde{|1\rangle}$  (dashed line) vs  $\sqrt{2}p$ ; (h): real part of the momentum wave-functions  $\text{Re } \psi_+$  of  $\widetilde{|+\rangle}$  (solid line) and  $\text{Re } \psi_-$  of  $\widetilde{|-\rangle}$  (dashed line) vs  $\sqrt{2}p$ .

recovery process occurs when, given the state  $\varphi_0(x) \equiv \langle x | \widetilde{0} \rangle$ , the measurement gives a result within one of the error regions:  $R_n \equiv \sqrt{2} [2n - 3/2 - \beta, 2n - 1/2 - \beta]$ ,  $n = 0, 1, \dots$ . The corresponding intrinsic error probability  $P_{x,0}$  is equal to the one,  $P_{x,1}$ , which we would obtain starting from the state  $\varphi_1(x) \equiv \langle x | \widetilde{1} \rangle$  and considering the complementary error region. So we simply have

$$P_x = \sum_{n=0}^{\infty} \int_{\sqrt{2}(2n-\frac{3}{2}-\beta)}^{\sqrt{2}(2n-\frac{1}{2}-\beta)} dx |\varphi_0(x)|^2. \quad (44)$$

It is possible to prove that, under the condition  $r \gtrsim 3/2$ , allowing us to use the asymptotic expansion of the error function  $\int_x^{+\infty} dt e^{-t^2} = (2x)^{-1} e^{-x^2} [1 - O(x^{-2})]$ , we can write the following upper bound for  $P_x$ :

$$P_x \lesssim \frac{N^2}{\pi\sqrt{2}} e^{-(r+e^{2r}/2)} [e^{-\alpha^2} + \sum_{m=1}^{\infty} (\nu_{m-1} + \nu_m)^2]. \quad (45)$$

The recovery in the momentum space is instead performed by measuring the operator  $\hat{p}(\text{mod } \pi/\sqrt{2})$ . An intrinsic error in the recovery process occurs when, given the state  $\psi_+(p)$ , the measurement gives a result within one of the error regions  $R_n^+ \equiv (\pi/\sqrt{2}) [2n + 1/2, 2n + 3/2]$  ( $n = 0, \pm 1, \dots$ ), or, given the state  $\psi_-(p)$ , the measurement gives a result within one of the error regions  $R_n^- \equiv (\pi/\sqrt{2}) [2n - 1/2, 2n + 1/2]$  ( $n = 0, \pm 1, \dots$ ). The corresponding intrinsic error probabilities are given by

$$P_{p,\pm} = \sum_{n=-\infty}^{+\infty} \int_{R_n^\pm} dp |\psi_\pm(p)|^2. \quad (46)$$

Inserting Eq. (43) into Eq. (46) we get, after some algebra,

$$P_{p,\pm} \simeq \frac{2}{\pi} \frac{N^2}{N_\pm^2} e^{-r} \left[ K_{0,0}^\pm \sum_{m=0}^{\infty} \nu_m^2 + 2 \sum_{m>m'=0}^{\infty} \nu_m \nu_{m'} K_{m,m'}^\pm \right], \quad (47)$$

where

$$K_{m,m'}^\pm \equiv \sum_{n=-\infty}^{+\infty} \int_{R_n^\pm} dp \exp(-e^{-2r} p^2) (1 \pm \cos \sqrt{2} p) \cos[2\sqrt{2} p(m - m')]. \quad (48)$$

Again, the mean intrinsic error probability  $\bar{P}_e$ , averaged over all possible qubit encoded states, satisfies the inequality  $\bar{P}_e \lesssim P_{max} = \max\{P_x, P_{p,+}, P_{p,-}\}$ . However, in the present trapped qubit scheme, in a large and significant region of parameters, it is  $P_{p,+} \simeq P_{p,-} \equiv P_p \gg P_x$  so that we can take as upper bound for  $\bar{P}_e$  simply the quantity  $P_p$ .

Let us therefore study the behavior of this upper bound for the intrinsic error probability in the case of system parameters corresponding to a typical experimental cavity QED situation. As we have seen, the amplitude  $\alpha$  of the cavity mode coherent state and the squeezing parameter  $r$  the ion CM position are the relevant parameters to study, and they should be as large as possible. However, as in the preceding scheme, we have derived our approximate codeword states by making some assumptions and therefore  $\alpha$  and  $r$  cannot be freely chosen. A first limitation comes from the Lamb-Dicke limit. In practice this implies that during all the process of generation of the comb-like state the ion has to remain localized within a region smaller than  $\lambda_c$  so that the linearization of the optical potential is valid. We can roughly impose  $|\bar{x} \pm \Delta x| \lesssim \lambda_c/8$ , where  $\bar{x}$  is the ion mean position and  $\Delta x$  is its mean position spread. Using Eqs. (38), (39) and (42), we can see that the ion comb-like state  $\varphi(x)$  is substantially confined in the interval  $\sqrt{2}[2m_- - \beta, 2m_+ - \beta]$ , where  $m_\pm \equiv \max(\alpha^2/2 \pm \alpha/\sqrt{2}, 0)$ . Using this fact, we can see that the Lamb-Dicke limit implies

$$(2m_+ - \beta) \frac{2\xi}{k_c} \leq \beta \frac{2\xi}{k_c} \leq \frac{\lambda_c}{8}, \quad (49)$$

which is equivalent to require

$$\beta \leq \frac{\pi}{8\xi} \equiv \beta_{\max}, \quad \alpha \leq \frac{\sqrt{1+4\beta}-1}{\sqrt{2}} \equiv \alpha_{\max}(\beta). \quad (50)$$

In order to reach the maximum value of  $\alpha$  we choose  $\beta = \beta_{\max}$  so that

$$\alpha \leq \alpha_{\max}(\beta_{\max}) = \frac{\sqrt{1 + \pi/2\xi} - 1}{\sqrt{2}} \equiv \alpha_{\max}. \quad (51)$$

Therefore we have found an “optimal” value  $\beta_{\max}$  for  $\beta$ , and a corresponding upper bound  $\alpha_{\max}$  for  $\alpha$  imposed by the adoption of the Lamb-Dicke approximation. Moreover the Lamb-Dicke limit has to be satisfied also by the ion CM state at the beginning, and this implies a condition on the squeezing parameter  $r$  which is roughly given by  $r > 3/2$ .

Finally, the large detuning approximation imposes another limitation on  $\alpha$ . In fact, this condition reads  $\alpha \lesssim \delta/2g_0$  and using the condition for having a comb-like state  $k = 1/2$ , implying  $\delta = 2\xi g_0^2/\omega_a$ , we get

$$\alpha \leq \alpha'_{\max} \equiv \sqrt{\frac{\hbar}{20M\omega_a^3}} g_0 k_c. \quad (52)$$

To summarize, the adopted approximations imply the conditions  $r \gtrsim 3/2$ ,  $\alpha \leq \alpha''_{\max} \equiv \min(\alpha_{\max}, \alpha'_{\max})$  and  $\beta = \beta_{\max}$ . However, despite these constraints, one can find typical experimental situations in which these bounds are satisfied and one gets an interestingly low value for the estimated intrinsic error probability, suggesting therefore that also the present trapped qubit scheme can be used for the implementation of the CV encoding of Ref. [3]. For example, considering the case of a trapped  $Ca^+$  ion (with  $\lambda_0 \simeq 1\mu m$ ), if we choose experimentally realistic values such as  $\omega_a = 1.6$  Mhz,  $g_0 = 70$  MHz, one gets  $\alpha''_{\max} \simeq 1.8$  corresponding to  $\beta = \beta_{\max} \simeq 2.9$ . The same results for  $\alpha''_{\max}$  and  $\beta_{\max}$  are obtained also for a  $Ba^+$  ion (with  $\lambda_0 \simeq 0.87\mu m$ ) choosing  $\omega_a = 0.63$  Mhz,  $g_0 = 26.5$  MHz, or for a  $Hg^+$  ion (with  $\lambda_0 \simeq 0.79\mu m$ ) choosing  $\omega_a = 0.52$  Mhz,  $g_0 = 22$  MHz. In correspondence of these values for  $\alpha$  and  $\beta$ , and choosing  $r = 3/2$  one can derive that  $P_x \lesssim 2 \times 10^{-5}$  and  $P_{p,+} \simeq P_{p,-} \equiv P_p \simeq 2.4\%$ , so that the mean intrinsic error probability  $\bar{P}_e \lesssim 2.4\%$ . In particular, the chosen values of  $\alpha$  and  $r$  imply a *success probability*  $\mathcal{P}(x_0 = 0) \simeq 13.1\%$  according to Eq. (40). The corresponding approximate codewords are just the ones displayed in Fig. 7 up to a spatial displacement  $x \rightarrow x + \sqrt{2}\beta$ .

Finally, we have also done a numerical study of  $P_x, P_{p,+}, P_{p,-}$  in the wider parameter region  $0 \leq \alpha \leq 5.5$  and for  $r = 1.5, 2, 3$ . As anticipated above it is  $P_x \ll P_p \simeq P_{p,+}, P_{p,-}$  so that the intrinsic error probability is practically determined by  $P_p$ . This upper bound  $P_p$  weakly depends on  $r$  and, in fact, it has the same behavior for  $r = 1.5, 2, 3$ , while it has a significant dependence upon  $\alpha$ . As expected, one has better results for increasing  $\alpha$  (see Fig. 8), even though, as we have seen above, one cannot take too large values for it because of the Lamb-Dicke and large detuning approximations employed here.

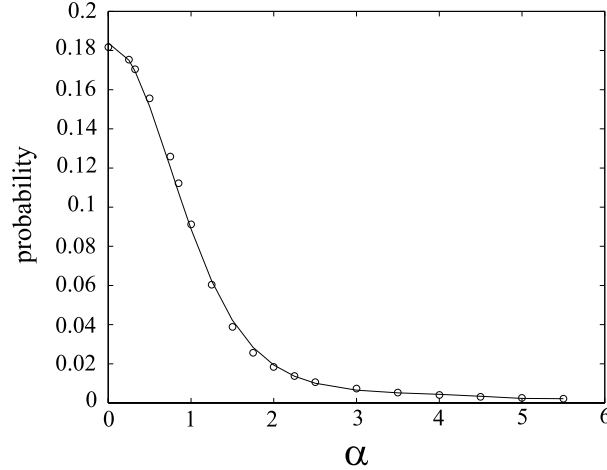


FIG. 8: Upper bound  $P_p$  for the mean error probability  $\bar{P}_e$  as a function of  $\alpha$  for  $r = 1.5$  (which is indistinguishable from that corresponding to  $r = 2$  and  $r = 3$ ). Numerical data (circles) are fitted by an exponential curve (line). We consider the extended interval  $0 \leq \alpha \leq 5.5$  even though, for typical experimental parameters, the use of the Lamb-Dicke limit implies that only the interval  $0 \leq \alpha \lesssim 2$  is experimentally accessible.

## V. CONCLUSION

For any quantum information processing to become a reality the task of providing adequate error correction needs to be fulfilled. As the quantum mechanical oscillator is a simply and prevalent model in the study of quantum mechanics,

it appears to be a natural test bed for such purposes. Thus we have discussed how to embed a qubit in a continuous quantum system, so that its redundancy can be used to correct errors which arise from unwanted interactions with the environment. In particular we have shown that ponderomotive interaction suffices to this end. Two schemes are proposed, a flying qubit scheme in which an atom released from a MOT crosses an optical cavity and a trapped qubit scheme in which a trapped ion within a cavity is considered.

In each of the proposed schemes we are able to show that sufficiently low values of the intrinsic error probability are effectively reachable so that the theoretical setting of [3] can be physically implemented with the current technology. For the sake of simplicity, throughout the paper we have considered protocols conditioned to a given result of a homodyne measurement of the intracavity field (the case corresponding to the outcome  $x_0 = 0$  to be specific). However in practical situations one has to consider a finite interval of acceptable measurement results. Then, it is possible to see that the success probability (for both schemes) is improved by enlarging the interval with the drawback of an increased error probability.

- 
- [1] See e.g. *Quantum Information Theory with Continuous Variables*, edited by A. K. Pati and S. L. Braunstein, Kluwer Academic Press (2002).
  - [2] S. Braunstein, Phys. Rev. Lett. **80**, 4084 (1998); S. Lloyd and J. E. Slotine, Phys. Rev. Lett. **80**, 4088 (1998).
  - [3] D. Gottesman, A. Kitaev, and J. Preskill, Phys. Rev. A **64**, 012310 (2001).
  - [4] B. C. Travaglione and G. J. Milburn, Phys. Rev. A **66**, 052322 (2002).
  - [5] B. C. Travaglione and G. J. Milburn, Phys. Rev. A **65**, 032310 (2002).
  - [6] S. Pirandola, S. Mancini, D. Vitali and P. Tombesi, Europhys. Lett. **68**, 323 (2004).
  - [7] S. Mancini and P. Tombesi, Phys. Rev. A **49**, 4055 (1994).
  - [8] A one-dimensional quantum oscillator or a one-dimensional free particle, which is a 1 – dim quantum oscillator with zero frequency.
  - [9] D. Gottesman, Phys. Rev. A **54**, 1862 (1996); A. R. Calderbank, E. M. Rains, P. W. Shor, and N. J. A. Sloane, Phys. Rev. Lett. **78**, 405 (1997).
  - [10] H. J. Metcalf and P. van der Straten, *Laser Cooling and Trapping* (Springer, 1999).
  - [11] D. F. Walls, Aust. J. Phys. **49**, 715 (1996); P. Storey, M. Collett, and D. F. Walls, Phys. Rev. Lett. **68**, 472 (1992).
  - [12] It is possible to make a direct and precise measurement of this intracavity quantity using a high finesse cavity whose input-output mirror transmittivity is controlled through fast electronics [13].
  - [13] M. S. Taubman, H. M. Wiseman, D. E. McClelland, and H. A. Bachor, J. Opt. Soc. Am. B **12**, 1792 (1995).
  - [14] J. Bjorkholm, R. Freeman, A. Ashkin, and D. Pearson, Phys. Rev. Lett. **41**, 1361 (1978).
  - [15] D. Leibfried, R. Blatt, C. Monroe, and D. Wineland Rev. Mod. Phys. **75**, 281 (2003).
  - [16] J. McKeever, J. R. Buck, A. D. Boozer, A. Kuzmich, H.-C. Nagerl, D. M. Stamper-Kurn, and H. J. Kimble Phys. Rev. Lett. **90**, 133602 (2003).
  - [17] G.R. Gunthorlein et al., Nature **414**, 49 (2001); A.B. Mundt et al., Phys. Rev. Lett. **89**, 103001 (2002).
  - [18] S. Mancini D. Vitali, and P. Tombesi, Phys. Rev. A **61**, 053404 (2000).
  - [19] S. Mancini, V. I. Man'ko, and P. Tombesi, Phys. Rev. A **55**, 3042 (1997).
  - [20] S. Bose, K. Jacobs, and P. L. Knight, Phys. Rev. A **56**, 4175 (1997).
  - [21] D. F. Walls and G. J. Milburn, *Quantum Optics*, (Springer, Berlin, 1994).
  - [22] R. M. Wilcox, J. Math. Phys. **8**, 962 (1967).